

Electrohydrodynamic instability of ion-concentration shock wave in electrophoresis

Rahul Gaur and Supreet Singh Bahga*

Department of Mechanical Engineering, Indian Institute of Technology Delhi, Hauz Khas, New Delhi 110016, India

(Received 7 March 2017; published 19 June 2017)

Capillary electrophoresis techniques often involve ion-concentration shock waves in an electrolyte solution, propagating under the effect of an external electric field. These shock waves are characterized by self-sharpening gradients in ion concentrations and electrical conductivity that are collinear with the electric field. The coupling of electric field and fluid motion at the shock interface sometimes leads to an undesirable electrohydrodynamic (EHD) instability. Using linear stability analysis, we describe the motion of small-amplitude disturbances of an electrophoretic shock wave. Our analysis shows that the EHD instability results due to the competition between destabilizing electroviscous flow and stabilizing electromigration of the shock wave. The ratio of timescales corresponding to electroviscous flow and electromigration yields a threshold criterion for the onset of instability. We present a validation of this threshold criterion with published experimental data and also describe the physical mechanism underlying the EHD instability of the electrophoretic shock wave.

DOI: [10.1103/PhysRevE.95.063109](https://doi.org/10.1103/PhysRevE.95.063109)**I. INTRODUCTION**

Capillary electrophoresis techniques such as capillary zone electrophoresis (CZE) [1], isotachopheresis (ITP) [2,3], and field amplified sample stacking (FASS) [4] are widely employed in analytical chemistry for separation and in some cases preconcentration of ionic species from sample mixtures. All electrophoresis techniques are based on differential migration of ionic species in an electrolyte solution under the effect of a strong electric field [1–3]. The differential migration of ions in electrophoresis usually leads to stationary or propagating gradients in ion concentrations and electrical conductivity, which can be described as concentration waves [5–8].

In binary electrolytes, consisting of one cationic and one anionic species, the gradients in electrical conductivity remain stationary under the effect of an electric field [7,8]. Conductivity gradients in binary electrolytes occur in FASS and such gradients broaden with time due to diffusion [4]. On the other hand, presence of three or more ionic species with comparable concentrations can lead to strongly nonlinear propagating concentration waves such as shock and expansion waves [5–9]. The nonlinearity in the electromigration of ions results from the coupling of ion concentrations with the local electric field due to the Ohm's law [5,6]. Unlike the diffusive gradients in a binary electrolyte, shocks waves in ion concentrations (and conductivity) remain sharp due to the balance of electromigration and diffusion at the shock interface [10]. Such self-sharpening concentration shocks are employed in ITP [2,3,9,11,12]—a widely used electrophoresis technique—to separate and preconcentrate ionic species. In ITP, ionic species are focused between two corresponding shock waves, which prevent the species from diffusing into the adjoining zones. This enables focusing of ionic species in narrow zones leading to amplification in their concentration.

To generate a single shock wave in ITP, electric field is applied across an interface between a leading electrolyte (LE) containing high electrophoretic mobility LE ions and a trailing electrolyte (TE) containing low-mobility TE ions [3], as shown

in Fig. 1. Both LE and TE contain a common counterionic species to ensure electroneutrality. If the electric field is applied such that the LE ions move in front of the TE ions, nonlinear electromigration leads to sharpening of the interface between LE and TE, resulting in a propagating shock wave [7,8]. Across the shock wave, a steep conductivity gradient is established. Typically, ITP and other electrophoresis experiments are performed by applying an axial electric field of $O(1\text{--}10\text{ kV m}^{-1})$ in microcapillaries with diameter of $O(10\text{--}100\text{ }\mu\text{m})$ [3]. While such strong electric fields are necessary for faster analysis and improving the detection sensitivity, high electric fields also lead to undesirable phenomenon of electrohydrodynamic instability (EHD) [13,14].

In this paper, we focus on the EHD instability of concentration shocks, which arise in nonlinear electrophoretic processes, such as ITP. EHD instability of the electrophoretic shock results from the coupling of electric field and fluid motion at the shock interface due to the presence of a sharp conducting gradient [13]. The gradient in electric field associated with the gradient in conductivity leads to accumulation of free charge at the shock interface. This free charge in turn couples with the local electric field to apply a destabilizing electric body force on the fluid. Shock instability is undesirable in ITP, because it causes asymmetry of the shock interface and focused sample zones, leading to uncertainty in sample quantification [13,14]. The detrimental effects of EHD instability of ITP shock were observed by Persat *et al.* [13] in their experiments on sample splitting at a channel bifurcation using ITP. Persat *et al.* observed that for electric fields of $O(10\text{ kV m}^{-1})$ EHD instability of ITP shock leads to an asymmetry in sample focusing and correspondingly uncertain splitting behavior at the channel bifurcation.

While EHD instability due to collinear conductivity gradient and electric field has been widely analyzed using linear stability analysis [15–18], the existing studies are limited to a stationary interface in a binary electrolyte separating high and low conductivity zones. The stability analysis for a stationary interface is not directly applicable to an electrophoretic shock wave because, unlike a stationary conductivity gradient in binary electrolyte, the shock wave also migrates under the effect of electric field. Therefore, in addition to the electric

*bahga@mech.iitd.ac.in

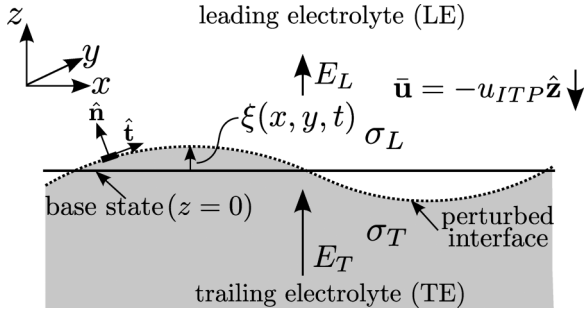


FIG. 1. Schematic of a shock wave in ITP separating zones of high-conductivity leading electrolyte (LE) and low-conductivity trailing electrolyte (TE). The conductivity of LE and TE zones is σ_L and σ_T , respectively ($\sigma_L > \sigma_T$). We analyze the EHD instability in a frame of reference moving along with the shock wave. In this reference frame, the shock in its base state is stationary at $z = 0$ and the base-state flow is in the $-z$ direction. The stability of the shock is analyzed by modeling the dynamics of an arbitrarily perturbed shock interface $z = \xi(x, y, t)$.

body force on the fluid, the stability of the shock wave in electrophoresis is also affected by electromigration of the shock. In this paper, based on the example of a shock wave in ITP, we present a linear stability analysis of an electrophoretic shock wave. Based on our stability analysis, we show that the onset of EHD instability of shock wave is governed by the competition between destabilizing electric body force and stabilizing electromigration of the shock wave. In particular, we present a threshold criterion for the onset of instability and validate it with published experimental data. We also elucidate the physical mechanism underlying the instability of electrophoretic shock wave.

II. MATHEMATICAL MODELING

A. Shock wave in ITP

Figure 1 shows a schematic of a shock wave in ITP separating high-conductivity LE and low-conductivity TE zones in an unbounded domain. In the base state, the shock is parallel to the x - y plane. The LE and TE ions are positively charged and the electric is applied along the $+z$ direction. Therefore, the ITP shock also propagates along the direction of applied electric field. In ITP, the conductivity of the TE zone adapts to the conductivity of LE zone in a way that the speeds of LE and TE ions in their respective zones are equal to the shock speed [2,7]. As shown by Kohlrausch [2], the composition and conductivity of TE zone is solely dependent on the initial composition of the LE zone. The shock speed u_{ITP} is given by

$$u_{ITP} = \mu_L E_L = \mu_T E_T, \quad (1)$$

where μ and E denote electrophoretic mobility and local electric field normal to the shock wave, respectively. The subscripts L and T denote LE and TE zones, respectively.

Because the current density is uniform across the shock wave, from Ohm's law, we have $\sigma_L E_L = \sigma_T E_T$ [7]. Therefore, from Eq. (1) the ratio of conductivity (γ) and local electric field of LE and TE zones depend on the mobility of LE and TE

ions as

$$\gamma \equiv \frac{\sigma_L}{\sigma_T} = \frac{E_T}{E_L} = \frac{\mu_L}{\mu_T}. \quad (2)$$

For an ITP shock wave to exist, the mobility of LE ion must be higher than the mobility of TE ions, $\mu_L > \mu_T$ [2]. Therefore, from Eq. (2), the local electric field in TE zone is higher than that in the LE zone.

B. Governing equations

To model the response of ITP shock wave to small perturbations, we consider a surface coupled model wherein the coupling between fluid flow and electric body force occurs only at the interface separating LE and TE zones. That is, the free charge accumulates only at the ITP interface, whereas the bulk fluid remains electroneutral. The surface coupling approach has been widely employed for analyzing EHD instability of an interface separating two immiscible conducting fluids stressed with normal and tangential electric fields [15,19,20]. In the context of ITP, the thickness δ of self-sharpening interface separating LE and TE zones scales as $\delta \sim kT/(eE_L)$ [10], where k denotes the Boltzmann constant, T the temperature, and e the elementary charge. For typical electric fields of $O(10^3-10^4 \text{ V m}^{-1})$ the shock thickness $\delta \sim O(1-10 \mu\text{ m})$, which is much smaller than the amplitude of interface disturbances observed during the instability [13,14]. The assumption of sharp interface, however, limits our analysis to disturbances with wave numbers $k \ll \delta^{-1}$.

Next, we note that the disturbance of the ITP interface does not alter the conductivity of LE and TE zones. The conductivity of TE zone is governed only by the initial LE composition [2], which is a consequence of zero eigenvalue of the set of hyperbolic conservation laws governing electrophoretic transport of ions [8]. The Riemann invariant corresponding to the zero eigenvalue, termed as the Kohlrausch function, is given by

$$K(x, y, t) = \sum_{i=1}^N z_i c_i(x, y, t) \left(\frac{1}{\mu_i} - \frac{1}{\mu_{N+1}} \right) = K(x, y, 0), \quad (3)$$

for an electrophoretic system consisting of $N + 1$ species. The initial value of Kohlrausch function, $K(x, y, 0)$, is set by the spatially uniform LE. Taking the LE and TE ions as species $i = 1, 2$ and the counterionic species as species $N + 1 = 3$ in Eq. (3), we conclude that the concentration of LE and TE ions remains uniform whenever LE or TE zones displace each other due to the disturbance of ITP interface. The sharp ITP interface and uniform conductivity of LE and TE zones ensure that the surface coupling approach is reasonable for analyzing interface disturbances greater than the interface thickness.

The governing equations for fluid flow and electric field in the bulk fluid are same as those described previously by Melcher and coworkers for EHD instability of a sharp, stationary interface separating two conducting fluids [15,20]. Briefly, the incompressible fluid flow is modeled using the continuity equation,

$$\nabla \cdot \mathbf{u} = 0, \quad (4)$$

and Navier-Stokes equations for momentum conservation,

$$\rho \frac{\partial \mathbf{u}}{\partial t} + \rho \mathbf{u} \cdot \nabla \mathbf{u} = -\nabla p + \eta \nabla^2 \mathbf{u}. \quad (5)$$

Here \mathbf{u} , ρ , and η denote the velocity, density, and viscosity of the fluid, respectively. Note that Eq. (5) does not have an electric body force as the bulk solution is electroneutral and the coupling between fluid flow and electric field takes place only at the sharp ITP interface.

The local electric field \mathbf{E} is related to the conductivity (σ) and free charge density (ρ_f) by the charge conservation equation [21],

$$\frac{\partial \rho_f}{\partial t} + \nabla \cdot (\rho_f \mathbf{u} + \sigma \mathbf{E}) = 0. \quad (6)$$

In this equation, the terms $\rho_f \mathbf{u}$ and $\sigma \mathbf{E}$ correspond to convection and Ohmic currents, respectively. Moreover, for a linear dielectric medium with uniform permittivity (ϵ), the electric field and free charge density are related by the Gauss' law,

$$\nabla \cdot (\epsilon \mathbf{E}) = \rho_f. \quad (7)$$

From Eqs. (6) and (7), we note that the terms with ρ_f in Eq. (6) can be neglected provided that the time scale of interest is much larger than the charge relaxation time scale ϵ/σ . For electrophoretic systems with aqueous electrolytes having $\epsilon = 7.1 \times 10^{-10} \text{ F m}^{-1}$ and $\sigma \sim O(0.01\text{--}1 \text{ S m}^{-1})$, the charge relaxation time ϵ/σ is of order $0.1 \mu\text{s}$ or smaller. On the other hand, the electrohydrodynamic and electromigration time scales of interest are of order 1 ms or larger [21]. Therefore, for electrophoretic systems, the current continuity equation, Eq. (6), simplifies to the Ohm's law,

$$\nabla \cdot (\sigma \mathbf{E}) = 0. \quad (8)$$

Last, at moderate current densities the electric field is irrotational,

$$\nabla \times \mathbf{E} = 0. \quad (9)$$

This quasidelectrostatic assumption holds well for electrophoretic systems as the magnetic field produced due to conduction and displacement currents is negligible [22].

Equations (4), (5), (8), and (9) can be solved along with appropriate boundary conditions and jump conditions at the sharp shock interface. Far away from the interface as $z \rightarrow \pm\infty$ the velocity and electric field perturbations vanish. At the shock interface with unit normal vector $\hat{\mathbf{n}}$ pointing toward the LE zone and tangent $\hat{\mathbf{t}}$, continuity of velocity leads to

$$[\mathbf{u}] \cdot \hat{\mathbf{n}} = 0 \quad \text{and} \quad [\mathbf{u}] \cdot \hat{\mathbf{t}} = 0. \quad (10)$$

Here $[f]$ denotes the value of a physical quantity f at the shock interface in the LE zone minus the value in the TE zone. The jump conditions for normal and shear stress balance are given by

$$\hat{\mathbf{n}} \cdot [\mathbf{T} - \rho \mathbf{u}\mathbf{u}] \cdot \hat{\mathbf{n}} = 0 \quad \text{and} \quad \hat{\mathbf{t}} \cdot [\mathbf{T} - \rho \mathbf{u}\mathbf{u}] \cdot \hat{\mathbf{n}} = 0, \quad (11)$$

where $\mathbf{T} = -p\mathbf{I} + \eta(\nabla \mathbf{u} + \nabla \mathbf{u}^T) + \epsilon \mathbf{E}\mathbf{E} - \epsilon \mathbf{E} \cdot \mathbf{E} \mathbf{I}/2$ is the stress tensor, \mathbf{I} is a unit tensor, and ϵ is the dielectric permittivity. In the current work, we assume that the electrolytes are linear dielectrics with equal and spatially uniform

dielectric permittivity. Finally, the continuity of current and the irrotationality of electric field at the shock interface yield

$$[\sigma \mathbf{E}] \cdot \hat{\mathbf{n}} = 0 \quad \text{and} \quad \hat{\mathbf{n}} \times [\mathbf{E}] = 0. \quad (12)$$

C. Linear stability analysis

We analyze the stability of ITP shock to small perturbations over a base state shown schematically in Fig. 1. In the base state the ITP shock is parallel to the x - y plane and is moving with a constant speed u_{ITP} , given by Eq. (1), in the $+z$ direction in a quiescent aqueous medium. For analytical simplicity, we consider the dynamics of the ITP shock in a reference frame moving along with the shock. In this frame of reference, the shock is stationary in the base state at $z = 0$ and the fluid is moving with velocity $\bar{\mathbf{u}} = -u_{\text{ITP}}\hat{\mathbf{z}}$. Because the conductivity of the TE zone is lower than that of the LE zone, the local electric field drops across the ITP interface. Therefore, from the Gauss law, in the base state a negative charge exists at the shock interface. For an undisturbed interface, the electric body force due to coupling of this charge with the base-state electric field is balanced by the base-state pressure \bar{p} . Using Eq. (11), the normal stress-balance at the ITP interface in the base state yields,

$$[\bar{p}] = \frac{1}{2}[\epsilon \bar{E}^2]. \quad (13)$$

Here, the overbar indicates the base state quantities.

To analyze the linear stability of the system over this base state, we introduce the following perturbation variables (with primes):

$$\begin{aligned} \mathbf{u}(x, z, t) &= \bar{\mathbf{u}} + \mathbf{u}'(x, z, t), & p &= \bar{p} + p', \\ \mathbf{E} &= \bar{\mathbf{E}} + \mathbf{E}'(x, z, t). \end{aligned} \quad (14)$$

Because the current system has rotational symmetry about the z axis, without loss of generality, we have confined our analysis to perturbations that are independent of y . Here, we note that the conductivity of the LE and TE zones is not affected when the shock interface is perturbed, that is, $\sigma = \bar{\sigma}$. Substituting the perturbation variables in the governing equations, Eqs. (4)–(9), and linearizing the resulting equations yields

$$\nabla \cdot \mathbf{u}' = 0, \quad (15)$$

$$\rho \frac{\partial \mathbf{u}'}{\partial t} - \rho u_{\text{ITP}} \frac{d\mathbf{u}'}{dz} = -\nabla p' + \eta \nabla^2 \mathbf{u}', \quad (16)$$

$$\nabla \cdot (\sigma \mathbf{E}') = 0, \quad (17)$$

$$\nabla \times \mathbf{E}' = 0. \quad (18)$$

Similarly, the boundary and interface jump conditions can be linearized over the base state.

To solve the linearized equations for perturbation variables, we perform normal modes analysis by assuming perturbation variables of the form $f'(x, z, t) = \hat{f}(z)\exp(st - ikx)$. By eliminating pressure from Eq. (16) using Eq. (15) we obtain a linear ordinary differential equation (ODE) for the z component of perturbation velocity \hat{w} ,

$$\left(D^2 - k^2 - \frac{\rho s}{\eta} + \frac{\rho u_{\text{ITP}} D}{\eta} \right) (D^2 - k^2) \hat{w}(z) = 0, \quad D \equiv \frac{d}{dz}. \quad (19)$$

Next, noting that the conductivity σ is uniform in LE and TE zones, from Eqs. (17) and (18) we obtain an ODE for the x component of perturbation electric field \hat{E}_x ,

$$(D^2 - k^2)\hat{E}_x(z) = 0. \quad (20)$$

Equations (19) and (20), along with the boundary and interface conditions, define an eigenvalue problem with growth rates s as the eigenvalues and \hat{w} and \hat{E}_x as the eigenfunctions. The general solutions of Eqs. (19) and (20) are of the form

$$\hat{w}(z) = \begin{cases} A_L e^{-kz} + B_L e^{q_L z}, & z > 0 \\ A_T e^{kz} + B_T e^{q_T z}, & z < 0 \end{cases} \quad (21)$$

$$\hat{E}_x(z) = \begin{cases} C_L e^{-kz}, & z > 0 \\ C_T e^{kz}, & z < 0 \end{cases} \quad (22)$$

where

$$v = \frac{\rho u_{ITP}}{2\eta}, \quad q_L = -v - q, \quad q_T = -v + q, \text{ and}$$

$$q = \left(\frac{\rho s}{\eta} + k^2 + v^2 \right)^{1/2}.$$

These solutions obey the boundary conditions at $z \rightarrow \pm\infty$ provided $q > v$. Knowing \hat{w} , the perturbation pressure \hat{p} can be obtained from Eq. (16),

$$\hat{p} = \frac{1}{k^2} [\eta(D^2 - k^2) - \rho s + \rho u_{ITP} D] D \hat{w}. \quad (23)$$

To solve for the growth rate s , we apply the interface jump conditions given by Eqs. (10)–(12) and relate the six unknown constants A_L, A_T, B_L, B_T, C_L , and C_T . Assuming an arbitrary interface perturbation given by $z = \xi(x, t) = \hat{\xi} \exp(st - ikx)$ and evaluating the jump conditions, Eqs. (10)–(12), at $z = 0$ we get

$$[\hat{u}] = 0, \quad [\hat{w}] = 0, \quad (24)$$

$$[\hat{p}] = \epsilon [\bar{E} \hat{E}_z] + 2\eta \left[\frac{\partial \hat{w}}{\partial z} \right], \quad (25)$$

$$-\frac{\partial \hat{\xi}}{\partial x} \epsilon [\bar{E}^2] = \epsilon [\bar{E} \hat{E}_x] + \eta \left[\left(\frac{\partial \hat{u}}{\partial z} + \frac{\partial \hat{w}}{\partial x} \right) \right], \quad (26)$$

$$[\sigma \hat{E}_z] = 0, \quad (27)$$

$$[\hat{E}_x] + \frac{\partial \hat{\xi}}{\partial x} [\bar{E}] = 0. \quad (28)$$

Here, \hat{u} denotes the x component of perturbation velocity and \hat{E}_z denotes the z component of perturbation electric field.

Because the shock wave moves due to fluid flow and electromigration, the kinematic condition at the interface can be written as

$$\frac{\partial \hat{\xi}}{\partial t} = \mu_L \hat{E}_z + \hat{w}|_{z=0^+} = \mu_T \hat{E}_z + \hat{w}|_{z=0^-}. \quad (29)$$

Note that the ITP condition $\mu_L/\mu_T = \sigma_L/\sigma_T$ ensures that Eq. (29) is consistent with the interface jump condition Eq. (27).

D. Dispersion relation

Substituting the general solution given by Eqs. (21) and (22) in the interface jump conditions, Eqs. (24)–(29), we obtain six homogeneous linear algebraic equations for the coefficients A_L, A_T, B_L, B_T, C_L , and C_T . This set of equations has a nontrivial solution provided that the determinant given by Eq. (A1) in the Appendix is zero. This yields the desired dispersion relation given by Eq. (30). In the dispersion relation, Eq. (30), we have used three timescales associated with viscous momentum diffusion (τ_v), electroviscous flow (τ_{ev}) resulting from the balance between the viscous and electric stresses [20], and electromigration of shock (τ_{em}). Therefore, Eq. (30) suggests that the stability characteristics of the shock depends on electroviscous flow, motion of shock wave due to electromigration, and dissipation due to viscous stresses.

$$\begin{aligned} & \left[(q' - 1)^2 - \left(\frac{\tau_v}{2\tau_{em}} \right)^2 \right] \left[(q' + 1) + \frac{\tau_v}{\tau_{em}} \left(\frac{\gamma}{1 - \gamma^2} \right) \right] \\ & - q' \left(\frac{\tau_v}{\tau_{ev}} \right)^2 \left[\left(\frac{\tau_{ev}}{\tau_{em}} \right)^2 - s'^2 \right] \left[\frac{\tau_{ev}}{\tau_{em}} \left(\frac{1 - \gamma}{1 + \gamma} \right) - s' \right] = 0, \end{aligned} \quad (30)$$

where

$$\begin{aligned} s' &= s \tau_{ev}, \quad q' = \frac{q}{k} = \sqrt{1 + \left(\frac{\tau_v}{2\tau_{em}} \right)^2 + \frac{\tau_v}{\tau_{ev}} s'}, \\ \tau_v &= \frac{\rho}{\eta k^2}, \quad \tau_{em} = \frac{1}{k u_{ITP}}, \quad \tau_{ev} = \frac{2\eta}{\epsilon(E_L - E_T)^2}. \end{aligned} \quad (31)$$

1. Scaling analysis

The dispersion relation given by Eq. (30) relates the dimensionless growth rate s' with three dimensionless parameters: τ_v/τ_{ev} , τ_{em}/τ_{ev} , and $\gamma \equiv \sigma_L/\sigma_T$. Alternatively, this relation can be written by regrouping the dimensionless parameters as

$$s' = f \left(\frac{\tau_{ev}}{\tau_v}, \frac{\tau_v \tau_{ev}}{\tau_{em}^2}, \gamma \right), \quad (32)$$

where

$$\frac{\tau_{ev}}{\tau_v} = \frac{2\eta^2 k^2}{\rho \epsilon [E]^2} \text{ and } \frac{\tau_v \tau_{ev}}{\tau_{em}^2} = \frac{2\rho \mu_L^2}{\epsilon(\gamma - 1)^2}. \quad (33)$$

This regrouping of the dimensionless parameters is interesting because it shows that among the three dimensionless groups on which s' depends, only the first dimensionless group τ_{ev}/τ_v depends on the wave number k of perturbation and electric field. The other two dimensionless groups $\tau_v \tau_{ev}/\tau_{em}^2$ and γ depend solely on the properties of electrolyte solutions. Therefore, we can define dimensionless wave number as $k' = \sqrt{\tau_{ev}/\tau_v}$. For a given composition of electrolytes, the dependence of growth rate s' on wave number k and electric field E_L can be solely captured by varying the dimensionless wave number k' . Therefore, throughout this paper, we discuss the variation of s' versus k' .

III. RESULTS AND DISCUSSION

We now consider the individual effects of electroviscous flow, electromigration, and viscous dissipation on the stability

of ITP shock wave. First, we consider the limiting case of a stationary interface in a binary electrolyte separating two regions with high and low conductivity. Thereafter, we consider the stability of ITP shock wave and describe the role of electromigration. Based on the results of these two cases, we finally elucidate the mechanism of instability of the shock wave. For our calculations, we consider an ITP system with sodium as the LE ion, Bistris as the TE ion, and Hepes as the counter-ion. The LE is composed of 100 mM sodium hydroxide and 200 mM Hepes. Based on one-dimensional numerical simulations using the Stanford public release electrophoretic separation solver (SPRESSO) [23,24] along with ionic strength corrections [25], the TE zone behind the shock wave is composed of 72.48 mM Bistris and 172.5 mM Hepes. For this ITP system, numerical simulations predict that $\mu_L = 42.6 \times 10^{-9} \text{ m}^2 \text{ V}^{-1} \text{ s}^{-1}$, $\mu_T = 7.77 \times 10^{-9} \text{ m}^2 \text{ V}^{-1} \text{ s}^{-1}$, $\sigma_L = 0.5617 \text{ S m}^{-1}$, and $\sigma_T = 0.1024 \text{ S m}^{-1}$. Note that these values of mobilities and conductivities satisfy the ITP condition given by Eq. (2), $\mu_L/\mu_T = \gamma = 5.48$. For all the calculations related to linear stability analysis, we use values of physical parameters that are typical of aqueous solutions: $\rho = 1000 \text{ kg m}^{-3}$, $\eta = 1 \times 10^{-3} \text{ N s m}^{-2}$, and $\epsilon = 7.1 \times 10^{-10} \text{ F m}^{-1}$.

A. Stationary interface limit

We begin by considering the limiting case of a stationary interface separating zones of high and low conductivity in a binary electrolyte. Such an interface remains stationary under an applied electric field and does not propagate as an electrophoretic shock wave. The linear stability analysis of this case has been performed previously by Melcher and Smith [15] and Kath and Hoburg [20] assuming that the interface is sharp. In the absence of diffusion, their analyses predicted the stationary interface to be linearly unstable. The dispersion relation for binary electrolyte given by Melcher and Smith [15] and Kath and Hoburg [20] can be recovered from Eq. (30) by taking the electromigration timescale to be very large compared with other timescales, $\tau_{em} \gg \tau_v$ and $\tau_{em} \gg \tau_{ev}$. In this limit, electromigration does not affect the stability of the interface and Eq. (30) simplifies to the dispersion relation given by Kath and Hoburg [20],

$$q'(q' + 1)(q'^2 - 1) = \frac{\tau_v}{\tau_{ev}}, \quad q' = \sqrt{1 + \frac{\tau_v}{\tau_{ev}} s'}. \quad (34)$$

As shown by Kath and Hoburg [20], Eq. (34) predicts a positive real-valued growth rate for all wave numbers k and applied electric fields E_L . To illustrate this, we consider an example case of an interface separating two zones of a binary electrolyte with conductivity ratio $\gamma = 5.48$, which is equal to that for the ITP system under consideration. In Fig. 2(a), we present the variation of dimensionless growth rate s' of the interface corresponding to the most unstable mode versus dimensionless wave number k' of perturbation. The growth rate is real-valued and positive for all wave numbers, indicating that the stationary interface in a binary electrolyte is linearly unstable when diffusion is neglected.

To get an insight into the physical mechanism responsible for instability, in Fig. 2(b) we present the variation of ratio of timescales associated with viscous dissipation and

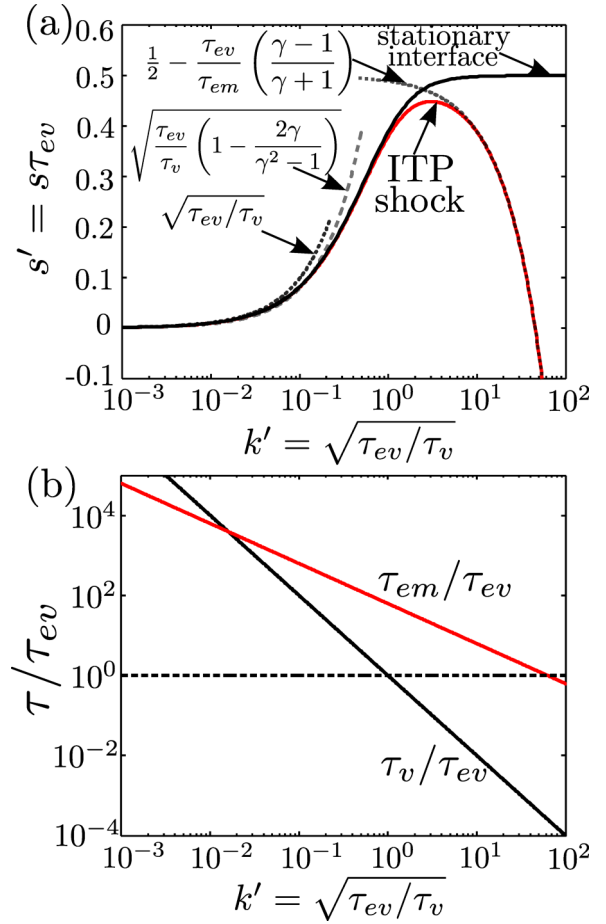


FIG. 2. Variation of growth rate s' of interface disturbances (a) and various timescales (b) with dimensionless wave number k' for a stationary conductivity gradient and an ITP shock wave. (a) Growth rate s' for the most unstable mode with varying wave number k' . The growth rate of disturbances in a stationary conductivity gradient and a shock wave compare well at low wave numbers. This is because, for low wave numbers ($k' \ll 1$) destabilizing electroviscous flow is dominant and electromigration is not prominent, as can be seen from the corresponding timescales in (b). For large wave numbers ($k' \gg 1$), the stabilizing electromigration of ITP shock dominates, resulting in negative growth rates.

electroviscous flow (τ_v/τ_{ev}) with the wave number. Because $\tau_{ev}/\tau_v \propto k^2$, at low wave numbers the viscous effects are negligible. In this inertia-dominated regime, taking the limit of $\tau_{ev}/\tau_v \ll 1$ in Eq. (34) yields $s' \simeq \sqrt{\tau_{ev}/\tau_v}$. Whereas, for large wave number disturbances where $\tau_{ev}/\tau_v \gg 1$, viscous effects dominate and in this limit the dispersion relation, Eq. (30), yields $s' \simeq 1/2$. As shown in Fig. 2(a), the growth rates for the limiting cases of small and large wave number limits agree well the exact values of growth rate. The results shown in Fig. 2 suggest that the electroviscous flow tends to destabilize the perturbations in the interface. On the other hand, the viscous stresses dissipate these disturbances, thereby limiting the growth rate for large disturbance wave numbers. However, in the absence of any restoring force, the sharp interface in binary electrolyte separating zones of high and low conductivity is linearly unstable.

B. Stability of ITP interface

Next, we analyze the stability of an ITP shock wave separating LE (sodium-Hepes) and TE (Bistris-Hepes) zones. To this end, we solve the dispersion relation given by Eq. (30) for varying dimensionless wave numbers k' of interface perturbation. In this case, the ratio of conductivity of both zones ($\sigma_L/\sigma_T = 5.48$) is same as that for the binary electrolyte case discussed in Sec. III A. However, in contrast to the binary electrolyte case, here the interface separating high-conductivity LE and low-conductivity TE zones propagates as a shock wave.

In Fig. 2(a), we present the dimensionless growth rate of interface perturbations corresponding to the most unstable mode versus the dimensionless wave number of perturbation. In addition, in Fig. 2(b) we present the variation of τ_v/τ_{ev} and τ_{em}/τ_{ev} for varying dimensionless wave numbers k' . Unlike the case of stationary interface in a binary electrolyte, here the electromigration timescale τ_{em} is comparable to the electroviscous timescale τ_{ev} , particularly for large wave numbers. Therefore, for large wave numbers disturbances of the shock wave, the growth rate differs significantly from that of the stationary interface. In particular, the growth rate of perturbations in the shock wave decreases at large wave numbers and eventually becomes negative. On the other hand, for low wave number perturbations, the growth rate is similar to that for a stationary conductivity gradient in a binary electrolyte, as shown in Fig. 2(a). The unstable mode with maximum growth rate among all wave-number perturbations is stationary and is expected to be dominant during the initial phase of instability. A comparative analysis of the results shown in Fig. 2 for stationary interface and shock wave suggests that the shock wave is stabilized at large wave numbers due to electromigration. This is because at large wave numbers the timescale for electromigration τ_{em} is smaller than the electroviscous timescale τ_{ev} .

1. Low wave-number limit

To gain further insight into the competition between electroviscous flow and electromigration on the EHD instability of electrophoretic shock wave, we consider the limiting cases of very low and high perturbation wave numbers. At low wave numbers $k' \ll 1$, Eq. (31) and Fig. 2(b) suggest that $\tau_v/\tau_{em} \gg 1$ and $\tau_{em}/\tau_{ev} \gg 1$. In this limit, assuming that the growth rate s' is real-valued, $q' \approx \tau_v/(2\tau_{em}) + \tau_{em}s'/\tau_{ev}$ from Eq. (31). Using these approximations, the dispersion relation given by Eq. (30) yields

$$s' \approx \sqrt{\frac{\tau_{ev}}{\tau_v} \left(1 - \frac{2\gamma}{\gamma^2 - 1} \right)} \text{ for } k' \ll 1. \quad (35)$$

Figure 2(a) shows that this approximation for the growth rate holds reasonably well up to $k' = 0.1$. Because $\tau_v/\tau_{ev} \gg 1$ when $k' \ll 1$, this limit corresponds to the inertial regime. Figure 2 also shows that, in the inertial regime, the behavior of growth rate on wave number is similar to that for a stationary conductivity gradient in a binary electrolyte. This is because, for small wave-number perturbations the timescale corresponding to electromigration of the shock wave is significantly larger than the electroviscous timescale ($\tau_{em}/\tau_{ev} \gg 1$).

Therefore, electromigration of shock wave does not affect the growth of small wave-number perturbations.

We note that to derive Eq. (35), we have assumed that the growth rate is real-valued. According to Eq. (35), this assumption is valid when the LE-to-TE conductivity ratio $\gamma > 1 + \sqrt{2}$. For a narrow range of LE-to-TE conductivity ratio, $1 < \gamma < 1 + \sqrt{2}$, computation of growth rates using the dispersion relation Eq. (30) shows that the most unstable mode at very low wave numbers is oscillatory with complex-valued growth rate. However, for $1 < \gamma < 1 + \sqrt{2}$, the mode with highest growth rate among all wave-number disturbances is still stationary with real-valued growth rate. Except for this narrow range of conductivity ratio, the growth rate for most unstable mode is always real-valued for all wave numbers and electric fields.

2. Large wave-number limit

In the limit of large disturbance wave number ($k' \gg 1$), Eq. (31) and Fig. 2(b) suggest that $\tau_v/\tau_{em} \ll 1$ and $\tau_{em}/\tau_{ev} \ll 1$ and $\tau_v/\tau_{ev} \ll 1$. In this limit, we can approximate q' from Eq. (31) as $q' \approx 1 + \tau_v s'/(2\tau_{ev})$. Substituting this value of q' in the dispersion relation, Eq. (30), and retaining only the leading order terms in $\tau_v s'/(2\tau_{ev})$ yields

$$s' \approx \frac{1}{2} - \frac{\tau_{ev}}{\tau_{em}} \left(\frac{\gamma - 1}{\gamma + 1} \right) \text{ for } k' \gg 1. \quad (36)$$

Figure 2(a) shows that this large wave-number approximation for the growth rate holds extremely well for $k' > 10$. Importantly, Eq. (36) predicts the threshold condition for the onset of instability,

$$\frac{\tau_{ev}}{\tau_{em}} < \frac{1}{2} \left(\frac{\gamma + 1}{\gamma - 1} \right). \quad (37)$$

That is, the instability sets in when the electroviscous velocity amplifies the disturbances faster than the rate as which electromigration restores them. Figure 2 clearly shows that the growth rate deviates from that of the stationary conductivity gradient when τ_{em} and τ_{ev} become comparable above $k' > 10$. Moreover, Fig. 2 shows that the stable regime results due to faster electromigration compared with electroviscous flow (small τ_{em}/τ_{ev}).

C. Physical mechanism of instability

The results presented in Sec. III B conclusively establish the destabilizing effect of electroviscous flow and the stabilizing effect of electromigration on the shock wave. To describe the physical mechanism of the instability of the shock wave, in Figs. 3(a) and 3(b) we present the eigenmodes \mathbf{E}' and \mathbf{u}' , respectively, corresponding to the most unstable state ($k' = 3.04, s' = 0.45$) shown in Fig. 2. Note that the perturbations in electric field and velocity are more prominent in the low-conductivity TE zone where the local electric field is higher than that in the high-conductivity LE zone.

In the base state, the shock is horizontal as depicted by the horizontal dotted line at $z = 0$. When the shock wave separating LE and TE zones is perturbed as shown in Fig. 3 (amplitude exaggerated for clarity) the local electric field decreases in the regions where low-conductivity TE displaces

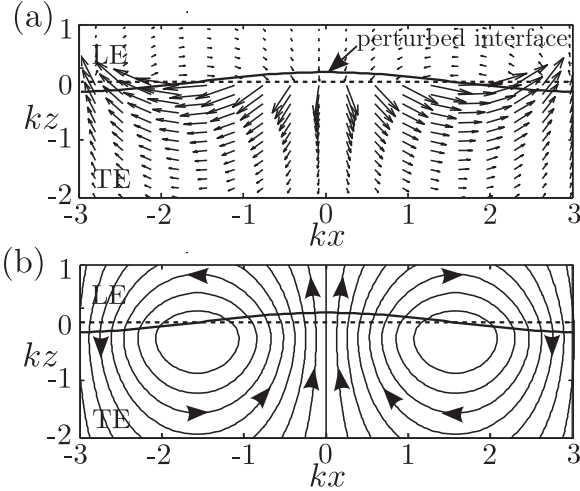


FIG. 3. Eigenmodes \mathbf{E}' and \mathbf{u}' corresponding to the most unstable state ($k' = 3.04$, $s' = 0.45$) of the ITP shock wave. (a) Perturbation electric field \mathbf{E}' resulting from the disturbance of shock wave. The local electric field decreases at locations where TE displaces LE and increases where LE displaces TE. The change in electromigration speed of the shock associated with this change in local electric field tries to restore the original shape of the shock wave. (b) Streamlines of the perturbation velocity \mathbf{u}' showing the destabilizing effect of electroviscous flow. The x and z coordinates have been nondimensionalized using the wave number k .

the high-conductivity LE. This can be seen from the downward pointing perturbation electric field \mathbf{E}' in Fig. 3(a) near $x = 0$ and $z = 0$. Therefore, the electromigration speed of shock wave, which is proportional to the local electric field, reduces in the regions where the TE displaces the LE. On the other hand, the local electric field increases where the LE displaces the TE and consequently the electromigration speed of the interface increases in these regions. Therefore, based on the perturbation electric field shown in Fig. 3(a) and the kinematic condition at the interface Eq. (29), we infer that electromigration tends to restore the original shape of shock wave.

In contrast to the restoring character of electromigration, the streamlines presented in Fig. 3(b) show that the electroviscous flow has a destabilizing effect. That is, perturbation of the shock wave leads to a cellular fluid motion that tends to further destabilize the interface, as shown in Fig. 3(b). The origin of such a cellular flow pattern remains to be explained. The electroviscous flow is driven by the perturbation in electric body force, which has two contributions due to the coupling of: (i) base-state interfacial charge and perturbation electric field and (ii) base-state electric field and perturbation interfacial charge [18]. For the situation presented in Fig. 3, the negative base-state interfacial charge couples with the perturbation electric field to apply a body force along the direction of interface perturbation. Also, considering the change in perturbation electric field across the interface in Fig. 3(a), we note that the perturbation interfacial charge is positive (negative) for interface displacement in the positive (negative) z direction. Consequently, the coupling of upward-pointing base-state electric field and perturbation interfacial charge also leads to an electric body force along the direction of

the interface disturbance. Therefore, the net effect of the perturbation electric body force is to drive a flow along the interface perturbation, resulting in a destabilizing cellular motion of the fluid as shown in Fig. 3(b).

D. Comparison with experiments

The linear stability analysis of an electrophoretic shock wave presented above suggests that the shock wave is unconditionally unstable. As shown in Fig. 2(a), for any value of applied electric field, there exists a range of disturbance wave numbers for which the growth rate is positive. In contrast, ITP experiments are routinely performed at high electric fields of order 1 kV m^{-1} without any instability [3,13]. This discrepancy can be explained by noting that ITP experiments are usually performed in microcapillaries and microchannels with thickness $d \sim O(10\text{--}100 \mu\text{m})$. In such microchannels the wave number of disturbance $k \sim d^{-1}$. For typical electric field of order 1 kV m^{-1} and $d \sim 10\text{--}100 \mu\text{m}$, Eq. (33) yields $\tau_{ev}/\tau_v \sim O(10\text{--}1000)$. That is, typical ITP experiments are performed in the viscous-dominated regime ($\tau_{ev}/\tau_v \gg 1$), where the linear stability analysis correctly predicts the ITP shock to be stable (see Fig. 2). In other words, in a typical ITP experiment the inertial limit with $\tau_{ev}/\tau_v \ll 1$ is not realized.

We note that in the current work, we have performed stability analysis of an electrophoretic shock wave in an unbounded domain. Therefore, the only length scale involved in our analysis is k^{-1} . In practice, electrophoresis experiments are performed in microchannels where the characteristic length scale is the width or depth of the microchannel, d . Therefore, the threshold criterion for the onset of instability, Eq. (37), derived for an unbounded system does not apply directly to practical electrophoresis systems. Nevertheless, based on our stability analysis we expect that the instability of shock wave sets in when the timescale of destabilizing electroviscous flow (τ_{ev}) becomes smaller than the timescale of restoring electromigration (τ_{em}). Therefore, replacing k with d^{-1} in the definition of τ_{em} in Eq. (31) we can analyze the experimental data on instability in terms of the following dimensionless number:

$$\frac{\tau_{ev}}{\tau_{em}} = \frac{2\eta\mu_L}{\epsilon(\gamma - 1)^2 E_L d}. \quad (38)$$

We expect the shock instability to set in for small values of τ_{ev}/τ_{em} when electroviscous flow dominates electromigration. Therefore, high values of conductivity gradient γ , electric field E_L , and channel thickness d would promote the instability. Whereas, increasing the viscosity η and mobility of LE μ_L would inhibit the instability.

To test this hypothesis we compare the above instability criterion with experimental data of Persat *et al.* [13]. Persat *et al.* performed detailed experimental visualization of ITP instability in a shallow microchannel with depth of $10 \mu\text{m}$ for varying electric field. In their anionic ITP experiments, LE was Tris hydrochloride (100 mM, pH = 8.0) and TE was Tris Hepes (100 mM, pH = 8.0). For this ITP system, our numerical simulations predict that $\mu_L = -68.47 \times 10^{-9} \text{ m}^2 \text{ V}^{-1} \text{ s}^{-1}$, $\mu_T = -15.91 \times 10^{-9} \text{ m}^2 \text{ V}^{-1} \text{ s}^{-1}$, and $\gamma = \mu_L/\mu_T = 4.3$ (same as the measured value [13]). Persat *et al.* [13] reported

their experimental data in terms of average electric field $E_{av} \equiv (E_L + E_T)/2 = (\gamma + 1)E_L/2$. Their experiments showed that ITP shock wave becomes unstable around $E_{av} = -12 \text{ kV m}^{-1}$, while at lower electric field of $E_{av} = -2 \text{ kV m}^{-1}$ the shock is stable. Note that, here electric field values are negative because electric field is applied in the opposite direction when LE and TE ions are negatively charged. At average electric field E_{av} values of -2 and -12 kV m^{-1} , Eq. (38) yield $\tau_{ev}/\tau_{em} = 2.3$ and 0.39 , respectively. This agrees with our hypothesis that the electrophoretic shock becomes unstable only when τ_{ev} is smaller than τ_{em} . The exact threshold value of τ_{ev}/τ_{em} below which shock instability sets in would also depend on the geometry of microchannel. The threshold criterion can be obtained empirically or through numerical simulations; in this paper, we have obtained the threshold criterion for an unbounded domain.

IV. CONCLUSION

We have used linear stability analysis to describe the EHD instability of a concentration shock wave that arises in nonlinear electrophoresis processes, such as ITP. We have shown that EHD instability results from the competition between destabilizing electroviscous flow and restoring electromigration of the shock wave. In particular, we have obtained a threshold criterion for the onset of instability in terms of the ratio of timescales corresponding to electroviscous flow and electromigration. We have also elucidated the physical mechanism of instability and validated our results with published experimental data.

For our analysis, we have used an example of shock wave in ITP. However, concentration shocks exist in other electric-field driven transport processes such as electromigration-dispersion [5,6], shock-electrodialysis based water deionization [8,26], and concentration-polarization at microchannel and nanochannel interfaces [27]. The analysis presented in this paper can be extended to analyze stability of concentration shock waves in such processes. We note, however, that the physical mechanism proposed in this work for shock instability, based on the competition of electroviscous flow and electromigration of the shock, would be the same for the aforementioned processes.

ACKNOWLEDGMENTS

We acknowledge the financial support received from the Science and Engineering Research Board (SERB), Government of India, under Grant No. SERB/F/2665/2014-2015.

APPENDIX: DETERMINANT FOR THE DISPERSION RELATION

To obtain the dispersion relation given by Eq. (30), we substitute the general solution given by Eqs. (21) and (22) in the interface jump conditions, Eqs. (24)–(29). This yields six homogeneous linear algebraic equations for the coefficients A_L , A_T , B_L , B_T , C_L , and C_T . For a nontrivial solution, the determinant of the respective coefficients given by Eq. (A1) should be zero:

$$\begin{vmatrix} 2\eta k + \frac{\rho s}{k} + \rho u_{ITP} & 2\eta k + \frac{\rho s}{k} - \rho u_{ITP} & -2\eta q_L & 2\eta q_T & i\epsilon \bar{E}_L & i\epsilon \bar{E}_T \\ 2i\eta k + \frac{ik\epsilon[\bar{E}^2]}{s} & -2i\eta k & i\eta(k + \frac{q_L^2}{k}) + \frac{ik\epsilon[\bar{E}^2]}{s} & -i\eta(k + \frac{q_T^2}{k}) & \frac{\mu_L k \epsilon[\bar{E}^2]}{s} - \epsilon \bar{E}_L & \epsilon \bar{E}_T \\ 1 & -1 & 1 & -1 & 0 & 0 \\ k & k & -q_L & q_T & 0 & 0 \\ -\frac{ik[\bar{E}]}{s} & 0 & -\frac{ik[\bar{E}]}{s} & 0 & 1 - \frac{\mu_L k[\bar{E}]}{s} & -1 \\ 0 & 0 & 0 & 0 & \sigma_L & \sigma_T \end{vmatrix} = 0. \quad (\text{A1})$$

- [1] J. W. Jorgenson and K. D. Lukacs, *Science* **222**, 266 (1983).
 [2] P. Bocek, *Top. Curr. Chem.* **95**, 131 (1981).
 [3] S. S. Bahga and J. G. Santiago, *Analyst* **138**, 735 (2013).
 [4] R. Bharadwaj and J. G. Santiago, *J. Fluid Mech.* **543**, 57 (2005).
 [5] S. Ghosal and Z. Chen, *Bull. Math. Biol.* **72**, 2047 (2010).
 [6] Z. Chen and S. Ghosal, *Phys. Rev. E* **85**, 051918 (2012).
 [7] V. G. Babskii, M. Y. Zhukov, and V. Yudovich, *Mathematical Theory of Electrophoresis* (Consultants Bureau, New York, 1989).
 [8] S. S. Bahga, R. Moza, and M. Khichar, *Proc. R. Soc. A* **472**, 20150661 (2016).
 [9] S. S. Bahga and J. G. Santiago, *Electrophoresis* **33**, 1048 (2012).
 [10] D. A. Saville and O. A. Palusinski, *AIChE J.* **32**, 207 (1986).
 [11] G. Goet, T. Baier, and S. Hardt, *Lab Chip* **9**, 3586 (2009).
 [12] K. Kuriyama, H. Shintaku, and J. G. Santiago, *Electrophoresis* **36**, 1658 (2015).
 [13] A. Persat and J. G. Santiago, *New J. Phys.* **11**, 075026 (2009).
 [14] S. L. M. Harrison, Prediction of isotachophoresis steady-state zone position and analysis of zone behavior around a 180° turn, Ph.D. thesis, Washington State University, 2007.
 [15] J. R. Melcher and C. V. Smith, *Phys. Fluids* **12**, 778 (1969).
 [16] J. F. Hoburg and J. R. Melcher, *Phys. Fluids* **20**, 903 (1977).
 [17] J. C. Baygents and F. Baldessari, *Phys. Fluids* **10**, 301 (1998).
 [18] S. Sharan, P. Gupta, and S. S. Bahga, *Phys. Rev. E* **95**, 023103 (2017).
 [19] J. R. Melcher and W. J. Schwarz Jr, *Phys. Fluids* **11**, 2604 (1968).
 [20] G. S. Kath and J. F. Hoburg, *Phys. Fluids* **20**, 912 (1977).

- [21] A. Ramos, *Electrokinetics and Electrohydrodynamics in Microsystems* (Springer, New York, 2011), Vol. 530.
- [22] A. Castellanos, A. Ramos, A. Gonzalez, N. G. Green, and H. Morgan, *J. Phys. D: Appl. Phys.* **36**, 2584 (2003).
- [23] M. Bercovici, S. K. Lele, and J. G. Santiago, *J. Chromatogr., A* **1216**, 1008 (2009).
- [24] S. S. Bahga, M. Bercovici, and J. G. Santiago, *Electrophoresis* **33**, 3036 (2012).
- [25] S. S. Bahga, M. Bercovici, and J. G. Santiago, *Electrophoresis* **31**, 910 (2010).
- [26] A. Mani and M. Z. Bazant, *Phys. Rev. E* **84**, 061504 (2011).
- [27] T. A. Zangle, A. Mani, and J. G. Santiago, *Chem. Soc. Rev.* **39**, 1014 (2010).